

---

This is an electronic reprint of the original article.  
This reprint may differ from the original in pagination and typographic detail.

Liu, Wenqian; Markert, Frank; Giuliani, Luisa; Hostikka, Simo

## Analyzing the gas temperature of a hydrogen jet fire in a compartment with the Fire Dynamics Simulator

*Published in:*  
International Journal of Hydrogen Energy

*DOI:*  
[10.1016/j.ijhydene.2023.11.306](https://doi.org/10.1016/j.ijhydene.2023.11.306)

Published: 31/01/2024

*Document Version*  
Publisher's PDF, also known as Version of record

*Published under the following license:*  
CC BY-NC-ND

*Please cite the original version:*  
Liu, W., Markert, F., Giuliani, L., & Hostikka, S. (2024). Analyzing the gas temperature of a hydrogen jet fire in a compartment with the Fire Dynamics Simulator. *International Journal of Hydrogen Energy*, 53, 1097-1106. <https://doi.org/10.1016/j.ijhydene.2023.11.306>

---

This material is protected by copyright and other intellectual property rights, and duplication or sale of all or part of any of the repository collections is not permitted, except that material may be duplicated by you for your research use or educational purposes in electronic or print form. You must obtain permission for any other use. Electronic or print copies may not be offered, whether for sale or otherwise to anyone who is not an authorised user.



# Analyzing the gas temperature of a hydrogen jet fire in a compartment with the Fire Dynamics Simulator

Wenqian Liu<sup>a,\*</sup>, Frank Markert<sup>a</sup>, Luisa Giuliani<sup>a</sup>, Simo Hostikka<sup>b</sup>

<sup>a</sup> Department of Civil and Mechanical Engineering, Technical University of Denmark, Brovej 118, Kgs. Lyngby, 2800, Denmark

<sup>b</sup> Department of Civil Engineering, Aalto University, Raketijanaukio 4 A, Espoo, 02150, Finland

## ARTICLE INFO

Handling Editor: Dr. E.A. Veziroglu

### Keywords:

Hydrogen jet fire  
Gas temperature  
Sensitivity analysis  
Fluid Dynamic Simulator  
Lagrangian particles

## ABSTRACT

This study presents a method to simulate hydrogen jet fire using the Fire Dynamics Simulator (FDS). To avoid modeling an actual nozzle, high-speed Lagrangian particles released from a virtual nozzle are introduced to simulate released hydrogen. The capability of this FDS model to predict gas temperature is validated by comparing simulation results with five existing experiments in a rectangular steel compartment with an open end. The effects of relevant parameters prescribed in the FDS model on the gas temperature are also analyzed, including numerical parameters (auto-ignition exclusion zone, offset, particle count, and grid) and physical parameters (particle velocity, spray angle, and auto-ignition temperature). The results show that gas temperatures near the nozzle are sensitive to these parameters. Based on the grey relational analysis, the auto-ignition temperature is the least important parameter to predict gas temperatures, while the grid is the most significant parameter for gas temperatures near the ceiling.

## 1. Introduction

Hydrogen is regarded as an important clean fuel for vehicles owing to its high energy and zero carbon emissions. Hydrogen fuel is usually compressed and stored in a high-pressure tank with a pressure of up to 70 MPa in a hydrogen vehicle. To guarantee the safety of the utilization of hydrogen fuel cell vehicles (HFCVs), a thermal pressure relief device (TPRD) is applied to the hydrogen storage vessels, aiming to clear up a hydrogen storage vessel automatically in case of an HFCV accident.

The TPRD device is activated once the surrounding temperature rises to about 110 °C, causing hydrogen to be released from a tank with a small orifice. When the released hydrogen is ignited, a hydrogen jet fire or hydrogen cloud explosion is likely to happen. The probability of a jet fire event is almost twice as frequent compared to a cloud explosion event as reported by Lafleur et al. [1]. A hydrogen jet fire is expected to occur in the event of immediate ignition of the hydrogen released. A hydrogen gas cloud explosion may happen in the case of delayed ignition events, if the released hydrogen is mixed with sufficient air before ignition, resulting in an overpressure that can damage the surrounding facility and injure people [2,3]. These findings are showing that the hydrogen jet fire plays a crucial role in the HFCV accident.

Hydrogen air mixtures have a low ignition energy (0.019 mJ) at

stoichiometric conditions and a wide flammability range (4 %–75 % by volume of hydrogen) [4]. Upon ignition, hydrogen flames emit less heat radiation than hydrocarbon flames, due to the non-soot nature of hydrogen fuels, and the heat transfer mainly occurs as convection. In addition, the hydrogen released from a compressed vessel in open space diffuses rapidly due to its lower density. The hydrogen jet fire from high-pressure vessels has long flame lengths, as well as high velocity and flame temperature (around 1500 °C) [5]. This means that hydrogen fire accidents could have more severe consequences than traditional fuels.

In an HFCV, the pressure of the hydrogen storage tank is more than 1.9 times the ambient pressure, so the TPRD release is choked causing the released jet flow to be under-expanded and reach sonic velocity at the TPRD nozzle [6]. As the jet flow expands to the ambient pressure, the shockwaves and supersonic speed are present [7,8]. Thus, a high-momentum hydrogen jet fire is formed, once the hydrogen is released from a high-pressure storage vessel through a small-size nozzle and ignited immediately [9]. This particular incident predominantly occurs in the event of an HFCV fire caused by collision, battery fire, strong sunlight exposure, etc [10]. When an HFCV suffers a fire incident, the hydrogen gas is released through the triggered TPRD mounted on the hydrogen storage tank and ignited. The flame of the hydrogen jet fire will impinge on the floor when the TPRD is downwards, further

\* Corresponding author.

E-mail addresses: [weliu@dtu.dk](mailto:weliu@dtu.dk) (W. Liu), [fram@dtu.dk](mailto:fram@dtu.dk) (F. Markert), [lugi@dtu.dk](mailto:lugi@dtu.dk) (L. Giuliani), [simo.hostikka@aalto.fi](mailto:simo.hostikka@aalto.fi) (S. Hostikka).

<https://doi.org/10.1016/j.ijhydene.2023.11.306>

Received 5 September 2023; Received in revised form 17 November 2023; Accepted 26 November 2023

Available online 5 December 2023

0360-3199/© 2023 The Authors. Published by Elsevier Ltd on behalf of Hydrogen Energy Publications LLC. This is an open access article under the CC BY-NC-ND license (<http://creativecommons.org/licenses/by-nc-nd/4.0/>).

exacerbating the safety issues associated with hydrogen leakage in a vehicle. Hence, it is of great significance to study the behavior of hydrogen jet fire to provide some guidance for the safety assessment of HFCV fires.

The hydrogen jet fire resulting from leakage of high-pressure tanks is determined by released conditions, such as vessel pressure, mass flow rate, ventilation, and so on. Up to now, several tests have been performed to investigate the properties of hydrogen jet fire [11–13]; however, most of them are limited by difficulties in carrying out hydrogen jet fire tests, such as ingent costs and experimental safety. Thus, to fill gaps, alternative techniques, like computational fluid dynamic (CFD) simulation, have been applied for the investigation of the hydrogen jet fire, most of which are reported in Table 1.

The overview of previous works given in Table 1 indicates that CFD simulation is an efficient approach to analyzing hydrogen jet characteristics, such as flame temperature, heat flux, flame length, overpressure, and so on. Moreover, many CFD tools can be used to study hydrogen jets, such as ANSYS Fluent [14], OpenFoam [15], FLACS [16], etc. For instance, the shockwave and Mach disk of the hydrogen jet fire are capable of being simulated in ANSYS Fluent [17]. In Table 1, the temperature, fire flame, and heat transfer of the hydrogen jet can be predicted by CFD simulations. Furthermore, the CFD simulations allow for flexibility in altering boundary conditions, model geometry, and measurements, leading to a broad exploration and deeper understanding of the fire scenario.

However, the Fire Dynamics Simulator (FDS) has not been used for high-velocity hydrogen jet fire even though it is one of the most popular

fire software for engineers. Possible reasons for the lack of reported applications include its limitation to low-speed flows, which is a consequence of the used low Mach number formulation, and the adopted structured mesh system which makes it challenging to resolve the inflow of hydrogen nozzles. Nevertheless, in relation to an accurate simulation of fire propagation and the integration of the hydrogen safety analyses with more conventional building fire safety analyses, more common employment of FDS would be desirable, because of its specialization in simulating fire propagation, good documentation, and relatively short calculation time for fire simulations. Moreover, FDS is an open-source software providing low-cost options of high-performance computing for engineers. A user-friendly graphical user interface is commercially available (PyroSim). Thus, the aim of this study is to develop and validate the FDS model that can predict the gas temperature from a compressive hydrogen jet fire. As part of the model development, a grey relational analysis (GRA) is performed, highlighting the influence of several parameters and model assumptions on simulation results.

## 2. Numerical methodology

### 2.1. Numerical model

FDS is a CFD code that solves low Mach number combustion equations on a rectilinear grid over time. The flow solver is based on the Large Eddy Simulation (LES) method of turbulence, where the turbulent scales greater than the mesh size are solved explicitly, and the sub-grid scale phenomena are modeled using Deardorff eddy viscosity closure.

**Table 1**  
Summary of some hydrogen jet simulation.

Researches Ref.	Nozzle (mm)	Nozzle Direction	Initial conditions	Software	Measurements	Remark
Houf et al., 2009 [18]	5.08	Vertical	Velocity (448.2 m/s)	FUEGO	Centerline temperature	The predicted centerline temperature was sensitive to the inlet turbulent intensity between 5 % and 20 %.
Muthusamy et al., 2011 [19]	3.2, 6.4, 9.5	Horizontal	Tank pressure (200 bar)	FLACS	Flame temperature, Instantaneous total heat flux	The new CFD hydrogen jet fire model can predict the heat flux well when the release orifice is small.
Wang et al., 2014 [20]	5.08, 10, 20.9	Vertical, Horizontal	Tank pressure (104.8 bar, 32.99 bar, 59.8 bar)	FireFoam	Flame length, Radiant fraction, Flame temperature	The radiant fractions are more sensitive to the ground surface reflection than surface emissive power.
Keenan et al., 2017 [21]	3	Horizontal	Mass flow rate (0.045 kg/s)	OpenFoam, ANSYS-Fluent	Hydrogen volume fraction	Based on the hydrogen volume concentration along the jet centerline, OpenFoam performs marginally better than ANSYS-Fluent.
Xiao et al., 2018 [22]	5	Vertical	Mass flow rate (0.5486 g/s)	GASFLOW-MPL	Convection heat transfer, Thermal radiation	Heat losses of the combustion product significantly influence confined hydrogen fires.
Hussein et al. 2018 [23]	0.5, 2, 3.34	Vertical	Mass flow rate (0.299 kg/s, 0.107 kg/s, 0.0067 kg/s)	ANSYS-Fluent	Overpressure	The pressure peak in the ignited hydrogen release is two orders of magnitude larger than that in the un-ignited release.
Rian 2019 [24]	20.9, 52.5	Horizontal	Mass flow rate (1 kg/s, 7.5 kg/s)	KAMELEON-FIREEX-KFX	Gas temperature, Thermal radiation	The new CFD model can predict incident thermal radiation well in a large-scale hydrogen jet fire.
Cirrone et al. 2019 [7]	2	Horizontal	Tank pressure (900 bar)	ANSYS-Fluent	Radiative heat flux, Flame length	The predicted flame length has good agreement with the test data, and the simulated radiative heat flux followed the experimental result trend after 10s.
Cirrone et al. 2019 [25]	0.75, 1, 1.25	Vertical	Mass flow rate (0.33–0.64 g/s), Initial pressure (2–5 bar)	ANSYS-Fluent	Flame length, Radiative heat flux	The water vapor in the air has a large influence on the flame thermal radiation, causing a variation of up to 13 %.
Mashhadimoslem et al., 2020 [26]	12.75	Vertical	Fuel velocity (252.48–254.51 m/s)	ANSYS-CFX	Flame height, Incident radiation, Flame temperature	Hydrogen jet fire has a high maximum flame temperature and lower incident radiation compared with propane jet fire.
Hussein et al., 2021 [27]	0.5, 2, 3.34	0°, 30°, 45°, 90°	Tank pressure (700 bar)	ANSYS-Fluent	Gas temperature	The downward release of hydrogen contributed to a decrease in the temperature of a hot cloud under the ceiling.
Xia et al., 2022 [28]	4.57	Vertical	Mass flow rate (0.0011 kg/s)	ANSYS-Fluent	Flame lift-off distance, Coflow temperature	The flame lift-off distance increases with the decrease of the co-flow temperature.
Lv et al., 2023 [29]	2, 3, 4	Vertical	Mass flow rate (0.107 kg/s, 0.242 kg/s, 0.43 kg/s)	FLACS	Hydrogen concentration, Mass flow rate, Volume of a flame gas cloud, Flame temperature	A large nozzle diameter causes a large envelope of the flammable gas cloud (FGG), and the upward release decreases the volume of FGG outdoors.

The wall-adapting local eddy-viscosity (WALE) model was used for the near-wall eddy viscosity. Discretized equations were solved using explicit, second-order, kinetic energy conserving numerics. In this study, the simulations were performed using FDS version 6.7.9.

Combustion of gaseous hydrogen was modeled as a single-step, mixing-controlled reaction of hydrogen and air using the Eddy Dissipation Concept (EDC) method for the reaction rate. The radiation model was the Finite Volume Method (FVM) with 104 radiation angles for the angular discretization. A prescribed radiative fraction of the local heat release rate equal to 0.2 was used and the grey absorption coefficients for the water vapor were calculated as effective coefficients over a 0.1 m path length using a narrow-band model (RADCAL). Readers are referred to the FDS Technical Reference Guide for more details [30].

Due to the large difference between the fuel jet and room length scales, it was not possible to resolve the fuel stream using the CFD mesh. Instead, the hydrogen stream was modeled as a source of sub-grid scale, Lagrangian particles carrying the necessary mass flow and momentum [31,32]. The same approach has previously been used for modeling the release of aviation fuel from aircraft-impacts [33] showing that the high-speed (high-Mach number) effect is limited to the near vicinity of the fuel injection point. This region is not explicitly simulated here. In the region, where the mass and momentum exchange take place, gas velocities are below the 0.3 Mach number limit, which is considered a valid range of the solver. The governing equations and solution methods are presented in Ref. [30], so only the special aspects related to the use of Lagrangian particles in the hydrogen jet fire model are repeated in this paper.

### 2.1.1. Nozzle injection model

Lagrangian particles can be introduced in FDS via a nozzle as liquid droplets. The droplets are introduced into the FDS simulation on a section of a virtual spherical surface at a prescribed distance from the nozzle orifice. The initial spray is defined by the position and alignment of the nozzle, the opening angle of the spray, and the internal mass flow distribution within this angle, as well as the droplet properties, such as velocity and size distribution. The initial speed of droplets at the virtual surface is [34]:

$$u_{dro,0} = C\sqrt{\Delta P_n / \rho_{dro}} \quad (1)$$

where  $\rho_{dro}$  is the liquid fuel density;  $\Delta P_n$  is the pressure at which the nozzle is operating and  $C$  is a factor that accounts for friction losses in the nozzle, here adopted as 0.95. The initial droplet position within the spray cone is randomly selected from a Gaussian distribution [30,35]:

$$f(\varphi) = \exp\left[-\beta(\varphi/\varphi_{max})^2\right] \quad (2)$$

where  $\varphi_{max}$  is the opening half-angle of the spray ( $5^\circ$ ), and  $\beta$  is a spread uniformity parameter, by default  $\beta = 5$ . The droplet diameters  $D$  are randomly chosen from the cumulative volume distribution described by a combination of log-normal and Rosin-Rammle distributions [30]:

$$F_v(D) = \begin{cases} \frac{1}{\sqrt{2\pi}} \int_0^D \frac{1}{\sigma D'} \exp\left(-\left[\ln\left(\frac{D'}{D_{v,0.5}}\right)\right]^2 / 2\sigma^2\right) dD' & D' \leq D_{v,0.5} \\ 1 - \exp\left(-0.693(D/D_{v,0.5})^\gamma\right) & D' > D_{v,0.5} \end{cases} \quad (3)$$

$$\sigma = 2 / (\sqrt{2\pi} (\ln 2)^\gamma) \quad (4)$$

where  $D_{v,0.5}$  represents the median volumetric droplet diameter and  $\gamma$  is a distribution width parameter, adopted 2.4. In this study, the initial median droplet diameter was set to 1000  $\mu\text{m}$ .

### 2.1.2. Lagrangian particle model

The trajectory of a Lagrangian particle is controlled by the momentum conservation equation [30,34].

$$\frac{d}{dt} (m_d \vec{u}_d) = -\pi D'^2 \bar{\rho} C_d (\vec{u}_d - \vec{u}) \left| \vec{u}_d - \vec{u} \right| / 8 + m_d g \quad (5)$$

$$C_d = \begin{cases} 24/Re_d & Re_d < 1 \\ 24(0.85 + 0.15Re_d^{0.687})/Re_d & 1 < Re_d < 1000 \\ 0.44 & 1000 < Re_d \end{cases} \quad (6)$$

$$Re_d = \rho \left| \vec{u}_d - \vec{u} \right| D' / \mu \quad (7)$$

where  $Re_d$  is the droplet Reynolds number,  $m_d$  represents the particle mass;  $\vec{u}_d$  refers to the particle velocity;  $D'$  is the particle diameter;  $\vec{u}$  refers to the gas velocity in the vicinity of the particle;  $g$  is the gravity vector;  $C_d$  is the drag coefficient;  $\bar{\rho}$  is the gas density;  $\mu$  is the dynamic viscosity of air. The transfer of momentum between the droplets and the gas is depicted by a force term in the momentum equation, calculated by summarizing the drag terms induced by all particles in a given grid cell. In addition, the droplet temperature was calculated by solving an ordinary differential equation for droplet enthalpy, considering convective and radiative heat exchange and heat absorbed by evaporation. The evaporation rate was calculated using a mass-transfer number approach, transferring the hydrogen from the liquid to the gas phase.

## 2.2. Jet fire model

### 2.2.1. Description of validation test

Several hydrogen release tests were conducted at the University of South-Eastern Norway [36,37]. The experimental tests are carried out in a steel compartment with a dimension of 11.885 m  $\times$  2.24 m  $\times$  2.285 m (length  $\times$  width  $\times$  height). In this compartment, one steel wall opens (the exit wall), and the ventilation pipe is on the opposite wall of the exit wall, located 0.05 m from the ceiling with a 0.315 m outlet diameter. The insulation material thickness covering the walls and ceiling is 0.07 m. A steel table is used to imitate an HFCV with a dimension of 1.965 m  $\times$  0.73 m  $\times$  0.25 m (length  $\times$  width  $\times$  height). The hydrogen nozzle is mounted under the steel table. To detect the gas temperature under the hydrogen jet fire, thermocouples are mounted in this steel compartment, as shown in Fig. 1.

In all figures, ‘TT’ refers to the thermocouple. Five different hydrogen jet fire experiments are used to validate the CFD model. In these tests, the hydrogen is released with different initial tank pressure, ventilation, and jet duration, the parameters of these tests are shown in Table 2.

### 2.2.2. Computational setup

The computational domain and the placement of the fuel nozzle and steel table are shown in Fig. 2. The numerical domain has a dimension of 12 m  $\times$  2.24 m  $\times$  2.28 m (length  $\times$  wide  $\times$  height), and it was discretized with 0.04 m resolution. The effects of the numerical parameters are investigated in the sensitivity study.

Hydrogen gas condensates at temperatures below its boiling point of  $-253^\circ\text{C}$  at ambient pressure, so the initial temperature of droplets is prescribed as  $-260^\circ\text{C}$  to ensure the hydrogen is in a liquid state when they enter the simulation. An artificial auto-ignition temperature of  $250^\circ\text{C}$  was set in this FDS model to prevent the droplets from igniting immediately after being introduced, thus preventing combustion in the high-shear region near the nozzle. Because of the resolution constraints, this auto-ignition temperature is lower than the true hydrogen auto-ignition temperature, and it should be considered as a model parameter controlling fuel source stability and realism in the presence of simplified physics. To enable the ignition at a desired distance from the nozzle, a specific zone was defined where the auto-ignition temperature is not effective (auto-ignition temperature exclusion zone).

One-dimensional heat conduction was used to calculate the heat transfer to the steel walls at the solid boundaries. The surface layer

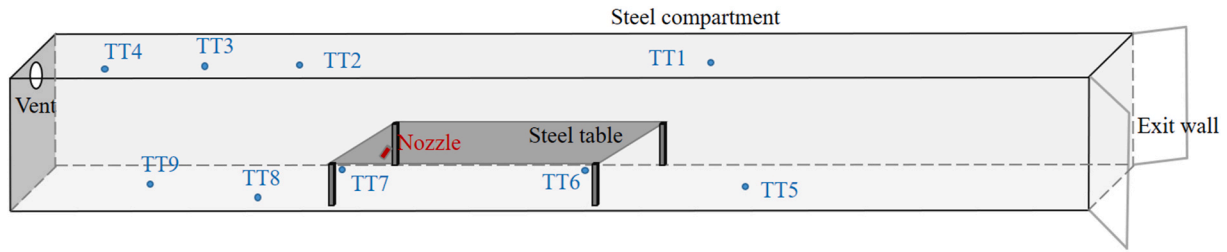


Fig. 1. Experimental setup showing the measurement points after [36].

**Table 2**  
Hydrogen jet fire parameters in experiments after [36,37].

Test No.	Air change per hour (1/h)	Initial tank pressure (bar)	Initial mass flow rate (g/s)	Blowdown duration (s)
1	6	698	7.4	500
2	10	690	7.3	500
3	10	357	4.1	500
4	6	360	4	500
5	6	357	13	367

material of the floor is the fire plate with a thickness of 70 mm. The wall has two material layers, one is steel material with a thickness of 5 mm, and another one is insulation material with a thickness of 70 mm. The thermal conductivities of the fire plate, steel, and insulation material are 0.05 W/(mK), 45.8 W/(mK), and 0.05 W/(mK), respectively. For the steel table, the exposed backing is prescribed to calculate the heat conduction through the whole thickness of the table.

### 3. Model validation

The temperatures registered by nine thermocouples in five experimental tests (referred to as Test1, ..., Test5) are compared with the corresponding predictions by five related FDS models (referred to as FDS1, FDS5). For TT2, only the results of two tests are available, due to problems that occurred to those thermocouples in the remaining three tests. The differences among these tests are the mass flow rate of the nozzle caused by different nozzle diameters and hydrogen tank pressure, as well as the volume flow rate of the ventilation. In Fig. 3, ‘TT’ refers to the thermocouple number, and the position of these sensors can be found in Fig. 1. Thermocouples TT1–TT4 are close to the ceiling of the steel compartment. The comparisons demonstrate good agreement between the FDS simulation and test results. In Test5, e.g., the maximum

measured temperature for TT3 is 324.2 °C, and 328.9 °C in the related FDS simulation, FDS5.

TT5 is behind the steel table and close to the ground and side wall. The measured and predicted temperature curves of TT5 are very similar. The maximum temperature of TT5 is less than 70 °C. TT6 and TT7 are under the steel table, the disparity between these two sensors is that TT6 is on the corner of the table and far away from the nozzle, while TT7 is close to the nozzle resulting in TT7 being more sensitive to the geometrical details of the hydrogen jet flame. The near-field turbulent fluctuations and dissipation of heat in the impingement region are very difficult to capture with a 4 cm mesh resolution. As a result, there are large differences in the TT7 temperatures. TT8 and TT9 are in front of the steel table, and TT8 is directly within the jet and TT9 is near the ventilation wall. For TT8, many simulations over-predict the peak temperature, especially Test5. For TT9, simulations of Tests 1–4 could predict the gas temperature, while the FDS5 underestimates.

Fig. 4 shows an image of the hydrogen jet flame in Test4 and, for comparison, a volumetric rendering of the instantaneous combustion heat release rate in simulation FDS4. The appearance (size and location) of the simulated flame of FDS4 is qualitatively similar to Test4, demonstrating that the Lagrangian particles can be used for modeling high-speed jets of low boiling-point flammable liquids, as long as the combustion related parameters are carefully chosen – and calibrated if necessary – to describe the details of the spray combustion, such as the initial high-shear region.

Fig. 5 displays the measured and predicted maximum temperatures for the five fire scenarios, with a total of 42 values extracted from Fig. 3. Temperature differences are observed in the region close to the nozzle and across the jet flame, registered by TT7 and TT8. In particular, TT8 in FDS5 highly overestimated the maximum temperature (approximately three times the experimental temperature increase). For positions outside the immediate flame region, the predicted results show good agreement with the test results, as shown by the fact that all other

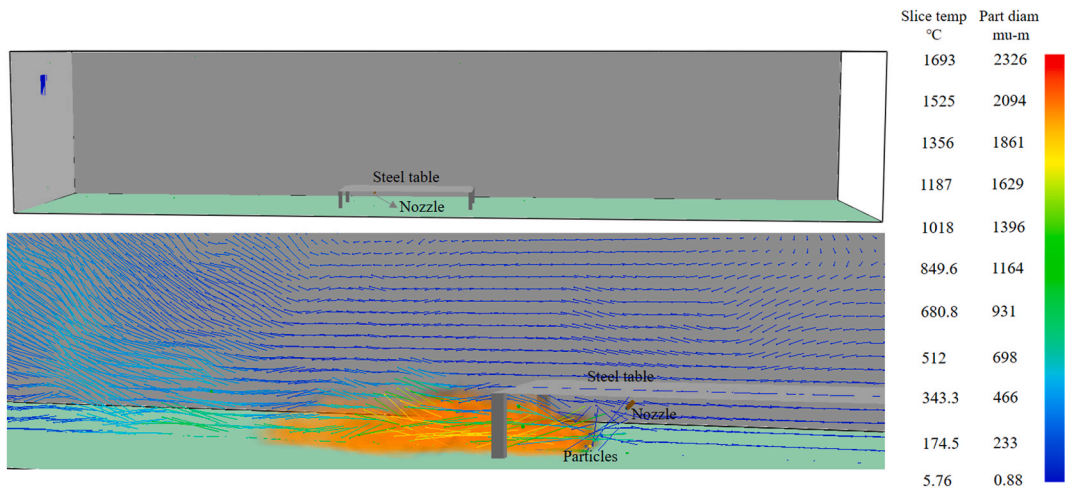


Fig. 2. FDS model of the experimental facility (top), and detailed visualization of the hydrogen jet flame (bottom), with instantaneous velocity vectors, gas temperature in °C, and particle sizes in μm.

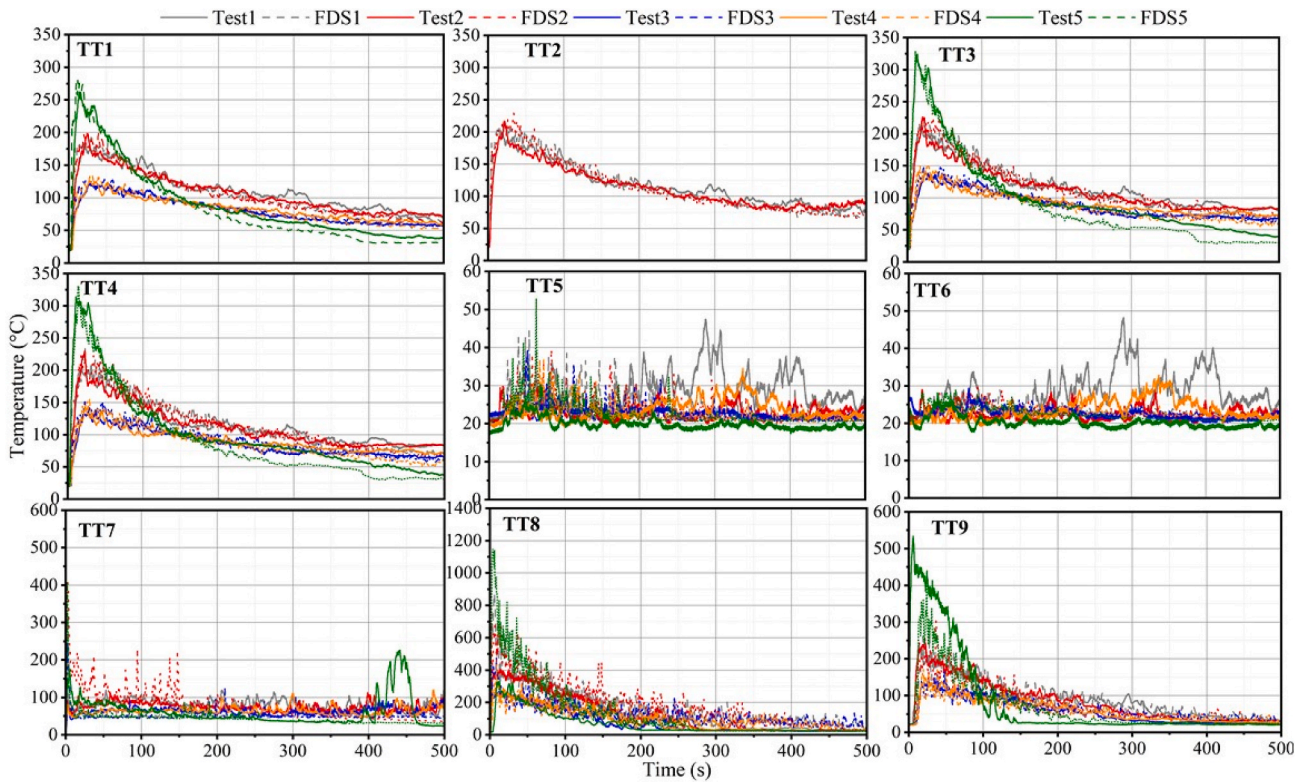
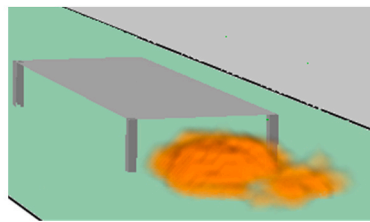


Fig. 3. Comparison of gas temperatures in FDS simulations and tests [36,37].



(1) Jet fire flame of Test4



(2) Volumetric rendering of instantaneous combustion heat release rate in simulation FDS4

Fig. 4. Comparison of the jet fire flame in the FDS simulation and test [36] under 60 s.

thermocouples lie very close to the dotted line, representing a perfect match between the measured and predicted temperature.

#### 4. Sensitivity study

##### 4.1. Sensitivity study introduction

The performance of the hydrogen jet fire model relies on several parameters, e.g., droplet position, droplet distribution, spray cone angle, etc. However, values of different parameters in this hydrogen jet fire model are assumed according to engineering judgment, test data, or literature. Since these values are not sure, it is necessary to conduct a sensitivity study on these input parameters within a reasonable range to pre-determine the significant parameters that can influence the numerical results a lot. This can provide guidance for engineers in similar issues and avoid wasting time on unnecessary calculations on such simulations.

In line with parameters in the Loughborough jet model [38] and FDS user guide [31], four numerical parameters (AEZ, OF, PPS, and CELL) and three physical parameters (PV, SA, and AIT) are selected in this study, and values of different parameters in the base case are shown in Table 3. Note that only one parameter value was changed in each

simulation of the sensitivity study, and a total of 29 simulation cases are investigated in the following analysis.

##### 4.2. Simulation results

To compare the simulation results with the test data, the deviation is introduced as Eq (8). The numerical value refers to the maximum temperature (°C) of each thermocouple sensor in FDS simulations, and the test value is the maximum temperature (°C) of each measurement point obtained in Test4.

$$\varepsilon = (\text{numerical value} - \text{test value}) / \text{test value} \quad (8)$$

Figs. 6 and 7 show the deviation between the maximum gas temperature in the simulation and test on each thermocouple sensor in different parameters. The horizontal axis indicates the position of different gas temperature sensors along the length (longitudinal direction) of the compartment, and the position of each measurement point is the same as in Fig. 1. For example, TT4 is close to the vent wall, TT5 nears the opening wall, and TT7 adjacents the nozzle. Owing to the test issues of TT2, the results of TT2 are not displayed in these two figures. The position of all sensors along the height and width of the compartment are not shown in Figs. 6 and 7. Details of the position of all sensors

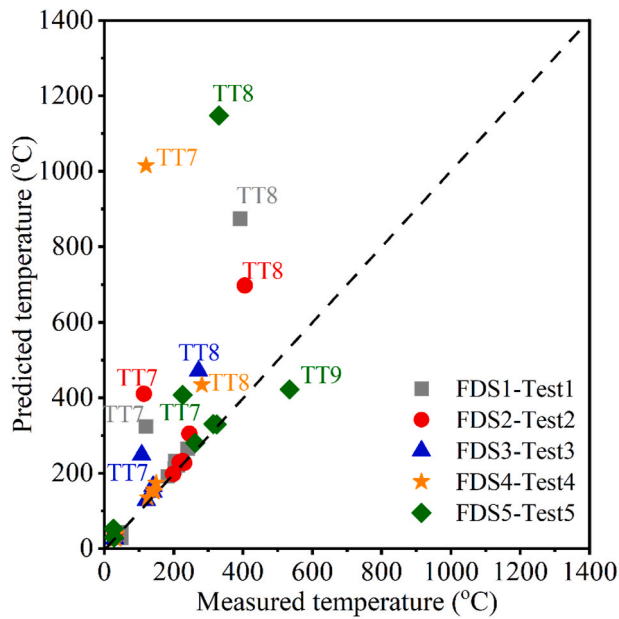


Fig. 5. A comparison of predicted and measured maximum temperature for the different fire scenarios in Tests 1–5.

can be found in section 2.2. Note that in Figs. 6 and 7, the deviation is reported in the range (–1, 1) and values outside this range are not exhibited.

In Fig. 6, the deviations of ceiling maximum gas temperature (TT1, TT3, and TT4) are almost equal to 0 when AEZ values change from 0.02 m to 0.18 m. For the maximum temperature of a sensor located in front of the hydrogen jet, TT8, AEZ is a significant parameter because deviations change a lot under different AEZ values. When it comes to the OF parameter, deviations of TT1, TT6, and TT5 mostly are not changed as the OF ranges between 0.03 m and 0.09 m, revealing that the maximum temperatures of the sensor located behind the nozzle are not affected by OF in a certain range. However, deviations vary a lot in TT9, TT3, and TT5, when the value of is larger than 0.09 m. This is because smaller OF could lead most of the hydrogen jet to ignite under the table, while larger OF results in the hydrogen jet fire running away from the table due to the higher impinged velocity, affecting the surrounding gas temperature.

Deviations of TT1, TT3, and TT4 are nearly identical and close to 0, in the instance that the PPS value changes from 5000 to 25000, demonstrating that the PPS has little influence on the ceiling gas temperature. The other sensors are impacted by the PPS to some extent. For instance, the deviations of TT8 are larger than 0.5 as PPS is prescribed as 5000, 10000, and 20000. Regarding TT6, deviations are far away to 0 when PPS is 5000, illustrating that PPS could be set comparatively larger to some extent to predict the gas temperature behind the table and close to the floor more accurately. With reference to the grid cells,

Table 3  
Parameters of the base case.

Parameter	Value	Description	
Numerical parameters	AEZ: AIT_EXCLUSION_ZONE	X1,X2,Y1,Y2,Z1,Z2 3.5 m,4.8 m,0.77 m,1.47 m,0 m,0.1 m (varied parameter is Z2, the upper boundary of AEZ)	Specify a volume in which ignition may occur
	OF: OFFSET	0.07 m	Distance of the droplet inflow surface from the nozzle
	PPS: PARTICLES_PER_SECOND	10000	Number of droplets inserted every second
Physical parameters	CELL	957600 cells (0.04 m × 0.04 m × 0.04 m for each cell)	The total grid cells of the model
	PV: PARTICLE_VELOCITY	200 m/s	Initial droplet velocity
	SA: SPRAY_ANGLE	5°	Opening half-angle of the jet cone.
	AIT:	250 °C	Auto-ignition temperature is a cell temperature at the beginning of the time step below which combustion does not occur.
	AUTO_IGNITION_TEMPERATURE		

deviations of the measured maximum gas temperatures among all sensors alter with the cell number variation, showing that mesh size plays a crucial role in the gas temperature, especially for these sensors near the nozzle.

In Fig. 7, deviations of most measured maximum gas temperatures fluctuate under different PV values, such as TT9, TT8, and TT5, expressing that the PV parameter can have impact on the gas temperatures. For the ceiling gas temperature, deviations slightly fluctuate around 0 under different values of SA and AIT within a certain range. And yet deviations of TT8 change a lot with various values of physical parameters. Again, it seems that TT8, being located only 1.67 m from the nozzle in the longitudinal direction, is more sensitive to parameters affecting the detailed appearance of the jet. With respect to the gas temperature behind the nozzle, deviations of TT6 are nearly the same no matter the variation of values in AIT and SA, while deviations of TT5 change noticeably when the SA is equal to 10°. In general, unlike PV, the deviation of each gas temperature changed a little under different SA and AIT, excluding TT7 and TT8. Hence, parameter PV plays a crucial role in gas temperature compared with SA and AIT.

In general, positions of measurements should be considered when selecting values of parameters in this model. Some guidance about simulating the ceiling gas temperature in the jet fire model is given here. An optimal value for AEZ:Z2 is suggested as 0.18 m, and either 0.03 m or 0.05 m is recommended for OF. For PPS, although it is available from 5000/s to 25000/s in this model, 5000/s is recommended for the simulation due to the calculation time. Smaller mesh sizes can be beneficial for the accuracy of the ceiling gas temperature. PV is suggested to be specified as 250 m/s, 7.5° is advised to be prescribed for SA, and AIT can be selected from the temperature range of 250 °C–450 °C.

#### 4.3. Grey relational analysis

Grey relational analysis (GRA) is one of the efficient ways to evaluate the influences of various parameters on some indicators [39]. GRA aims to measure the degree of correlation among parameters and indicators by giving a single grey relational grade (GRG) to each parameter. Hence, GRA has been applied in many fields, e.g., energy systems [39], city sustainability [40], manufacturing industries [41], and so on. In this study, the GRA [42,43] exemplified below is employed to evaluate the impact of numerical and physical parameters on the gas temperature under hydrogen jet fires.

The first step of improved GRA is to define the reference and comparative sequences. Herein, the gas temperature is set to the reference sequence, and numerical and physical parameters are set as the comparative sequences. Normalizing these sequences is the next step, based on the relationship between each comparative sequence and reference sequence, such as target value, smaller the better or larger the better [44] (see Eq. (9)). In this study, the reference sequence is normalized based on the desired value.

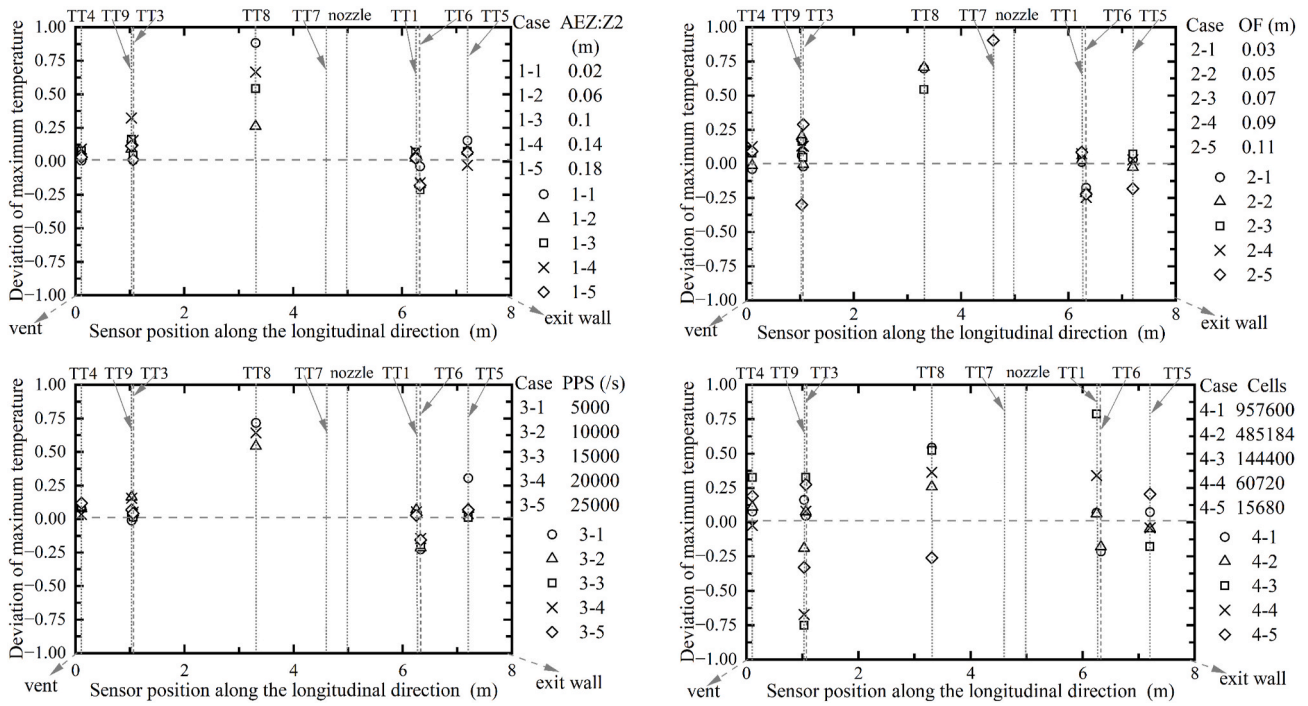


Fig. 6. The deviation between simulation and test results under different numerical parameters.

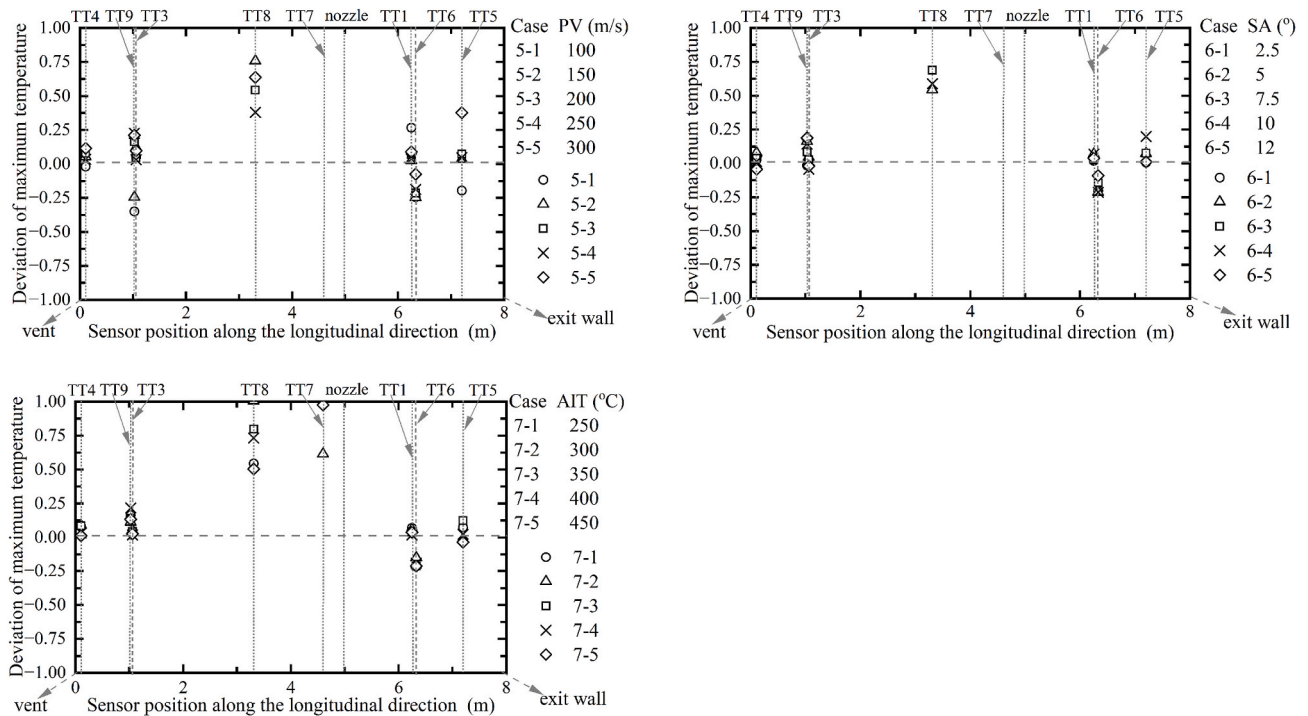


Fig. 7. The deviation between simulation and test results under different physical parameters.

$$x_i^*(k) = \begin{cases} 1 - \frac{|x_i(k) - OV|}{\text{MAX}\{\text{MAX}.x_i(k) - OV, OV - \text{MIN}.x_i(k)\}} & \text{desired value} \\ \frac{\text{MAX}.x_i(k) - x_i(k)}{\text{MAX}.x_i(k) - \text{MIN}.x_i(k)} & \text{smaller the better} \\ \frac{x_i(k) - \text{MIN}.x_i(k)}{\text{MAX}.x_i(k) - \text{MIN}.x_i(k)} & \text{larger the better} \end{cases} \quad (9)$$

Where  $x_i^*(k)$  is the normalized data of the  $i$ th parameter on the  $k$ th level in a comparative matrix. Herein, this comparative matrix contains 7 comparative sequences and 29 levels following the 29 simulation cases in section 4.2 of this study.  $\text{MAX}.x_i(k)$  and  $\text{MIN}.x_i(k)$  are the maximum and minimum values of each sequence, respectively.  $OV$  is the desired value, and the maximum gas temperature of each measurement obtained in the test is the desired value here.

Finally, the GRG is calculated by averaging the cosine value of fuzzy

membership and the Euclidean grey relational grade [39,43] as expressed by Eq. (10). Then Eq. (11) is used to calculate the cosine value of fuzzy membership and Eq. (12) is used to get the Euclidean grey relational grade.

$$\gamma_{ij} = \sqrt{\frac{\gamma_{1ij}^2 + \gamma_{2ij}^2}{2}} \tag{10}$$

$$\gamma_{1ij} = \frac{\sum_{k=1}^n x_i^*(k) y_j^*(k)}{\sqrt{\sum_{k=1}^n x_i^{*2}(k)} \sqrt{\sum_{k=1}^n y_j^{*2}(k)}}, i = 1, 2, 3, 4, 5, 6, 7; k = 1, 2, \dots, n. \tag{11}$$

$$\gamma_{2ij} = 1 - 2 \sqrt{\sum_{k=1}^n [w_k |\xi_{ij}(k) - 1|]^2} \tag{12}$$

Where,  $y_j^*(k)$  is the normalized data of the  $j$ th indicator on the  $k$ th level in a reference matrix.  $w_k$  is the weight coefficient obtained by the entropy weight method [45].  $\xi_{ij}(k)$  is the grey relational coefficient between  $x_i^*(k)$  and  $y_j^*(k)$  [46].

In light of the GRA method, the ranking of the calculated GRGs of seven parameters on each indicator is shown in Fig. 8. ‘TT1 – TT9’ refers to the maximum gas temperature obtained from 29 simulation cases in section 4.2. As for the gas temperature near the ceiling, e.g., TT1, TT3, and TT4, the largest GRG value appears in parameter CELL, showing that the mesh size is the most important parameter in the FDS model. This suggests that changing CELL could benefit the gas temperature in the FDS model to tend to the actual temperature. The subsequent crucial parameter in TT1, TT3, and TT4 is PV, OF, and AEZ, respectively. In addition, AIT is the least priority parameter in TT1, TT3, and TT4, since the GRG value of AIT is smallest compared with other parameters.

Concerning the influence of parameters on the gas temperature behind the nozzle injection and close to the floor, the most vital parameter in TT5 is PV with a GRG value of 0.9357, while CELL is the most essential parameter in TT6 with a GRG value of 0.9783. The next

vital parameter in TT5 and TT6 is CELL and PV, separately. In relation to the gas temperature close to the nozzle and under the steel table (TT7), the highest GRG value is equal to 0.9002 and the next greatest value is 0.8887, meaning that TT7 is mainly affected by the mesh size, followed by the AEZ parameter.

Pertaining to TT8, the most critical parameter is OF with a GRG of 0.9442, revealing that the OF parameter is decisive to the gas temperature across the jet flow and near the floor. This is due to the fact that the OF value controls the initial hydrogen droplet’s height in the simulation, resulting in different impingement velocities on the floor. Thus, TT8 is more sensitive to OF corresponding to a limited height range. The other device measuring the gas temperature in front of the nozzle and near the floor (TT9) is predominantly affected by CELL, with PV as the second most influential parameter. Furthermore, when referring to the least important parameter affecting the gas temperature, it’s obvious that the GRG of AIT is the lowest among other parameters in all indicators. As a result, when optimizing the hydrogen jet fire model in FDS, the prescribed appropriate parameters depend on which location is of interest to investigate the gas temperature. For instance, the CELL is first chosen for accurate gas temperature near the ceiling.

### 5. Conclusion

A numerical CFD model is proposed to simulate hydrogen jet fires in FDS. The high-speed hydrogen jet is modeled by applying Lagrangian particles that carry the necessary mass and momentum. The particles evaporate quickly producing a gas phase jet. The FDS model has been validated against the existing experimental work. The simulations of five validation scenarios showed that the modeling approach provides an accurate and efficient method for room-scale hydrogen jet fire consequence analysis. However, the accuracy of the gas temperatures around the nozzle in the FDS hydrogen jet model needs to be improved. This lack of accuracy can partly be ascribed to FDS limitations in simulating under-expanded flow with a high Mach number. Also, fine details of the nozzle and thermocouple placement and other geometrical factors may

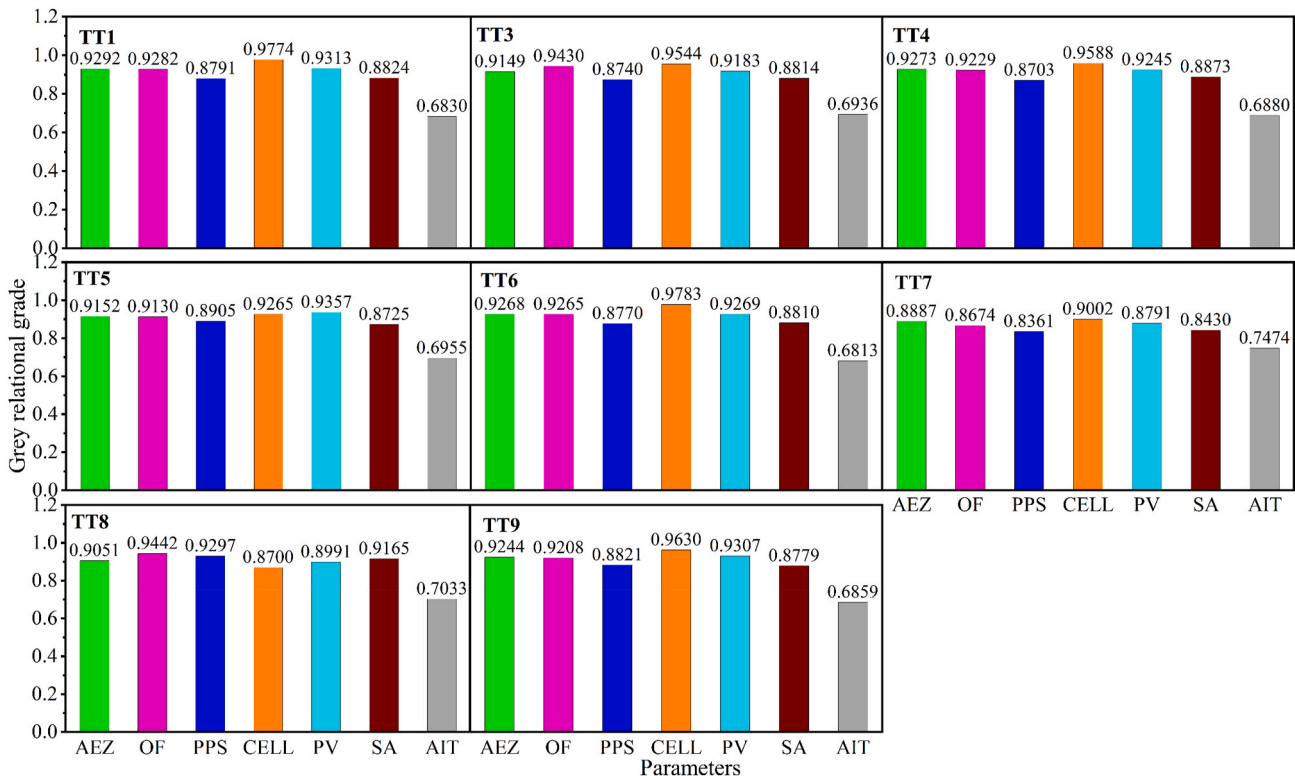


Fig. 8. Grey relational grades between parameters and gas temperatures.

have been modeled with less-than-necessary precision. Further validation of the Lagrangian particle description is needed with sufficiently detailed data from the jet flame region.

A grey relational analysis on four numerical and three physical parameters was performed to obtain the GRG between each parameter of the FDS model and the gas temperatures. Based on the GRA method, some guidance on the gas temperature accuracy improvement is given. The CFD gas phase resolution was found to be the dominant factor for the gas temperatures close to the ceiling and vent and under the steel table. As for the locations in the direct jet plume, the spray angle was also important in addition to the particle insertion offset and particle count. Details of the auto-ignition temperature were not important for the prediction of gas temperature in the FDS model. All in all, the prescribed appropriate parameters depend on the measurement position when optimizing the hydrogen jet fire model in FDS.

### Declaration of competing interest

The authors declare that they have no known competing financial interests or personal relationships that could have appeared to influence the work reported in this paper.

### Acknowledgments

The authors gratefully acknowledge the financial support provided by the Fuel Cells and Hydrogen 2 Joint Undertaking (now Clean Hydrogen Partnership) under Hy-tunnel CS Project [grant numbers 826193]. The authors gratefully acknowledge the support from the European Union's Horizon 2020 Research and Innovation program, Hydrogen Europe and Hydrogen Europe Research, the Finnish Fire Protection Fund (Palosuojelurahasto) [grant numbers VN/14165/2021], the Nordic Five Tech Alliance, as well as Otto Mønstedts Fond.

### References

- [1] Lafleur C, Bran-Anleu G, Muna AB, Ehrhart BD, Blaylock M, Houf WG. Hydrogen fuel cell electric vehicle tunnel safety study. In: SAND2017-11157; 2017. <https://doi.org/10.2172/1761273>. Sandia national laboratories albuquerque, New Mexico 87185 and livermore, California 94550.
- [2] Xie Y, Lv N, Huang Y, Wu D, Gong L, Yang X, Zeng Y. Comparative analysis on temperature characteristics of hydrogen-powered and traditional fossil-fueled vehicle fires in the tunnel under longitudinal ventilations. *Int J Hydrogen Energy* 2022;47:24107–18. <https://doi.org/10.2172/1761273>.
- [3] Liang Y, Pan X, Zhang C, Xie B, Liu S. The simulation and analysis of leakage and explosion at a renewable hydrogen refuelling station. *Int J Hydrogen Energy* 2019;44:22608–19. <https://doi.org/10.1016/j.ijhydene.2019.05.140>.
- [4] Alcock J, Shirvill L, Cracknell R. *Compilation of existing safety data on hydrogen and comparative fuels, 2-EIHP2. European integrated hydrogen project*; 2002. p. 1–15. May 2001.
- [5] Virtue B, Mohammadpour J, Salehi F, Abbassi R. Safety assessment of hydrogen jet fire scenarios within semi-confined spaces. *Fire* 2023;6(1):1–20. <https://doi.org/10.3390/fire6010029>.
- [6] Wang CJ, Wen JX, Chen ZB, Dembele S. Predicting radiative characteristics of hydrogen and hydrogen/methane jet fires using FireFOAM. *Int J Hydrogen Energy* 2014;39:20560–9. <https://doi.org/10.1016/j.ijhydene.2014.04.062>.
- [7] Cirrone DMC, Makarov D, Molkov V. Simulation of thermal hazards from hydrogen under-expanded jet fire. *Int J Hydrogen Energy* 2019;44(17):8886–92. <https://doi.org/10.1016/j.ijhydene.2018.08.106>.
- [8] Pan X, Yan W, Jiang Y, et al. Experimental investigation of the self-ignition and jet flame of hydrogen jets released under different conditions. *ACS Omega* 2019;4(7):12004–11. <https://doi.org/10.1021/acsomega.9b01214>.
- [9] Kessler A, Schreiber A, Wassmer C, Deimling L, Knapp S, Weiser V, et al. Ignition of hydrogen jet fires from high pressure storage. *Int J Hydrogen Energy* 2014;39:20554–9. <https://doi.org/10.1016/j.ijhydene.2014.05.116>.
- [10] Li ZY, Luo YY. Comparisons of hazard distances and accident durations between hydrogen vehicles and CNG vehicles. *Int J Hydrogen Energy* 2019;44(17):8954–9. <https://doi.org/10.1016/j.ijhydene.2018.07.074>.
- [11] Schefer RW, Merilo EG, Groethe MA, Houf WG. Experimental investigation of hydrogen jet fire mitigation by barrier walls. *Int J Hydrogen Energy* 2011;36(3):2530–7. <https://doi.org/10.1016/j.ijhydene.2010.04.008>.
- [12] Carboni M, Pio G, Mocellin P, et al. Experimental and numerical characterization of hydrogen jet fires. *Int J Hydrogen Energy* 2022;47(51):21883–96. <https://doi.org/10.1016/j.ijhydene.2022.05.010>.
- [13] Russo P, Marra F, Mazzaro M, et al. Spatial and radiative characteristics of large scale hydrogen jet-fires. *Chem Eng Trans* 2020;82:217–22. <https://doi.org/10.3303/CET2082037>.
- [14] Matsson JE. *An introduction to ANSYS fluent 2021*. SDC Publications; 2021.
- [15] CFD Direct. *OpenFOAM user guide*. 2015. <https://cfd.direct/openfoam/user-guide/>. [Accessed 17 November 2023].
- [16] As G. FLACS v10.9 user manual. Norway. Gexcon AS; 2019 (Web: <http://license.gexcon.com/FLACS-manual-external/html/index.html>). [Accessed 17 November 2023].
- [17] Takeno K, Yamamoto S, Sakatsume R, et al. Effect of shock structure on stabilization and blow-off of hydrogen jet flames. *Int J Hydrogen Energy* 2020;45(16):10145–54. <https://doi.org/10.1016/j.ijhydene.2020.01.217>.
- [18] Houf WG, Evans GH, Schefer RW. Analysis of jet flames and unignited jets from unintended releases of hydrogen. *Int J Hydrogen Energy* 2009;34(14):5961–9. <https://doi.org/10.1016/j.ijhydene.2009.01.054>.
- [19] Muthusamy D, Hansen OR, Middha P, Royle M, Willoughby D. *Modelling of hydrogen jet fires using CFD*. In: *The 4<sup>th</sup> international conference on hydrogen safety*; 2011. San Francisco, California; September 12–14.
- [20] Wang CJ, Wen JX, Chen ZB, Dembele S. Predicting radiative characteristics of hydrogen and hydrogen/methane jet fires using FireFOAM. *Int J Hydrogen Energy* 2014;39:20560–9. <https://doi.org/10.1016/j.ijhydene.2014.04.062>.
- [21] Keenan JJ, Makarov DV, Molkov VV. Modelling and simulation of high-pressure hydrogen jets using notional nozzle theory and open source code OpenFOAM. *Int J Hydrogen Energy* 2017;42:7447–56. <https://doi.org/10.1016/j.ijhydene.2016.07.022>.
- [22] Xiao J, Kuznetsov M, Travis JR. Experimental and numerical investigations of hydrogen jet fire in a vented compartment. *Int J Hydrogen Energy* 2018;43(21):10167–84. <https://doi.org/10.1016/j.ijhydene.2018.03.178>.
- [23] Hussein HG, Brennan S, Shentsov V, Makarov D, Molkov V. Numerical validation of pressure peaking from an ignited hydrogen release in a laboratory-scale enclosure and application to a garage scenario. *Int J Hydrogen Energy* 2018;43:17954–68. <https://doi.org/10.1016/j.ijhydene.2018.07.154>.
- [24] Rian KE. *Modelling and numerical simulation of hydrogen jet fires for industrial safety analyses: comparison with large-scale experiments*. In: *The 8<sup>th</sup> international conference on hydrogen safety*; 2019. Adelaide, South Australia; September 24–26.
- [25] Cirrone DMC, Makarov D, Molkov V. Thermal radiation from cryogenic hydrogen jet fires. *Int J Hydrogen Energy* 2019;44:8874–85. <https://doi.org/10.1016/j.ijhydene.2018.08.107>.
- [26] Mashhadimoslem H, Ghaemi A, Palacios A, Hossein Behroozia A. A new method for comparison thermal radiation on large-scale hydrogen and propane jet fires based on experimental and computational studies. *Fuel* 2020;282:118864. <https://doi.org/10.1016/j.fuel.2020.118864>.
- [27] Hussein H, Brennan S, Molkov V. Hydrogen jet fire from a thermally activated pressure relief device (TPRD) from onboard storage in a naturally ventilated covered car park. *Hydro* 2021;2(3):343–61. <https://doi.org/10.3390/hydrogen2030018>.
- [28] Xia Y, Verma I, Nakod P, Yadav R, Orsino S, Li S. Numerical simulations of a lifted hydrogen jet flame using flamelet generated manifold approach. *J Eng Gas Turbines Power* 2022;144(9):091009. <https://doi.org/10.1115/1.4055104>.
- [29] Lv H, Shen YH, Zheng T, et al. Numerical study of hydrogen leakage, diffusion, and combustion in an outdoor parking space under different parking configurations. *Renew Sustain Energy Rev* 2023;173:113093. <https://doi.org/10.1016/j.rser.2022.113093>.
- [30] McGrattan K, Hostikka S, Floyd J, McDermott R, Vanella M. *Fire dynamics simulator technical reference guide volume 1: mathematical model*. NIST special Publication 1018-1 sixth edition. 2022. <https://doi.org/10.6028/NIST.SP.1018>. . [Accessed 17 November 2023] (web:FDS-SMV Manuals (nist.gov)).
- [31] McGrattan K, McDermott R, Vanella M, Hostikka S, Floyd J. *Fire dynamics simulator user's guide*. 2022. <https://doi.org/10.6028/NIST.SP.1019>. NIST Special Publication 1019 Sixth Edition. . [Accessed 17 November 2023] (web:FDS-SMV Manuals (nist.gov)).
- [32] Liu WQ, Markert F, Giuliani L, Gaathaug AV, Hostikka S. Validation of a hydrogen jet fire model in FDS. Quebec, Canada; September 19–21. In: *The 10<sup>th</sup> international conference on hydrogen safety*; 2023. in press.
- [33] Sikanen T, Hostikka S. Numerical simulations of liquid spreading and fires following an aircraft impact. *Nucl Eng Des* 2017;318:147–62. <https://doi.org/10.1016/j.nucengdes.2017.04.012>.
- [34] Beji T, Ebrahim Zadeh S, Maragkos G, Mercier B. Influence of the particle injection rate, droplet size distribution and volume flux angular distribution on the results and computational time of water spray CFD simulations. *Fire Saf J* 2017;91:586–95. <https://doi.org/10.1016/j.firesaf.2017.03.040>.
- [35] Sikanen T, Vaari J, Hostikka S, Paajanen A. Modeling and simulation of high pressure water mist systems. *Fire Technol* 2013;50:483–504. <https://doi.org/10.1007/s10694-013-0335-8>.
- [36] Lach AW. *Hydrogen safety in confined spaces*. Doctoral thesis. In: Faculty of technology, natural sciences and maritime studies. University of South-Eastern Norway; 2022. p. 192–200. <https://hdl.handle.net/11250/3013137>.
- [37] Lach AW, Gaathaug AV. *Experimental data - hydrogen safety, thermal effects*. University of South-Eastern Norway; 2022. <https://doi.org/10.23642/usn.17695082.v1>. Dataset.
- [38] McGrattan K, McDermott R, Vanella M, Hostikka S, Floyd J. *Validation. Fire dynamics simulator technical reference guide, vol. 3*. NIST Special Publication 1018-3 Sixth Edition; 2022. p. 53–4. <https://doi.org/10.6028/NIST.SP.1018>. . [Accessed 17 November 2023] (web:FDS-SMV Manuals (nist.gov)).

- [39] Wu D, Zhou P, Zhou CQ. Evaluation of pulverized coal utilization in a blast furnace by numerical simulation and grey relational analysis. *Appl Energy* 2019;250:1686–95. <https://doi.org/10.1016/j.apenergy.2019.05.051>.
- [40] Yi P, Dong Q, Li W, Wang L. Measurement of city sustainability based on the grey relational analysis: the case of 15 sub-provincial cities in China. *Sustain Cities Soc* 2021;73:103143. <https://doi.org/10.1016/j.scs.2021.103143>.
- [41] Çaydaş U, Haşçalık A. Use of the grey relational analysis to determine optimum laser cutting parameters with multi-performance characteristics. *Opt Laser Technol* 2008;40(7):987–94. <https://doi.org/10.1016/j.optlastec.2008.01.004>.
- [42] Zhu R, Zhou P, Zhou C, Li J. Fuzzy grey relational analysis for influencing factors of heat transfer in a blast furnace hearth. *Ironmak Steelmak* 2018;45(10):899–906. <https://doi.org/10.1080/03019233.2017.1410967>.
- [43] Zuo W, Jiaqiang E, Liu X, Peng Q, Deng Y, Zhu H. Orthogonal experimental design and fuzzy grey relational analysis for emitter efficiency of the micro-cylindrical combustor with a step. *Appl Therm Eng* 2016;103:945–51. <https://doi.org/10.1016/j.applthermaleng.2016.04.148>.
- [44] Das A, Majumder A, Das PK. Detection of apposite PSO parameters using taguchi based grey relational analysis: optimization and implementation aspects on manufacturing related problem. *Procedia Mater Sci* 2014;6:597–604. <https://doi.org/10.1016/j.mspro.2014.07.074>.
- [45] Zou Z-h, Yun Y, Sun J-n. Entropy method for determination of weight of evaluating indicators in fuzzy synthetic evaluation for water quality assessment. *J Environ Sci* 2006;18(5):1020–3. [https://doi.org/10.1016/S1001-0742\(06\)60032-6](https://doi.org/10.1016/S1001-0742(06)60032-6).
- [46] Lin JL, Lin CL. The use of the orthogonal array with grey relational analysis to optimize the electrical discharge machining process with multiple performance characteristics. *Int J Mach Tool Manufact* 2002;42(2):237–44. [https://doi.org/10.1016/S0890-6955\(01\)00107-9](https://doi.org/10.1016/S0890-6955(01)00107-9).